Available online at www.sciencedirect.com
SCIENCE DIRECT
Carbon 44 (2006) 1496–1502
CARBON
www.elsevier.com/locate/carbon

Self-sensing of flexural damage and strain in carbon fiber reinforced cement and effect of embedded steel reinforcing bars

Sihai Wen, D.D.L. Chung *

Composite Materials Research Laboratory, University at Buffalo, State University of New York, Buffalo, NY 14260-4400, USA

Received 10 November 2005; accepted 5 December 2005
Available online 13 March 2006

Abstract

Self-sensing of flexural damage and strain in carbon fiber reinforced cement is attained by measuring the volume or surface resistance with the four-probe method and electrical contacts on the compression and/or tension surfaces. The oblique resistance (volume resistance in a direction between the longitudinal and through-thickness directions) increases upon loading and is a good indicator of damage and strain in combination. The surface resistance on the compression side decreases upon loading and is a good indicator of strain. The surface resistance on the tension side increases upon loading and is a good indicator of damage. The effectiveness for the self-sensing of flexural strain in carbon fiber reinforced cement is enhanced by the presence of embedded steel rebars on the tension side. For the same midspan deflection, the fractional change in surface electrical resistance is increased in magnitude, whether the surface resistance is that of the tension side or the compression side. The fractional change in resistance of the tension surface is increased by 40%, while the magnitude of the fractional change in resistance of the compression surface is increased by 70%, due to the steel.

Keywords: Carbon fibers, Carbon composites; Microcracking, Damage; Electrical properties, Strain effect; Cement; Electrical (electronic) properties, Elastic properties; Mechanical properties

1. Introduction

Cement reinforced with short carbon fibers has been shown to be able to sense its own strain [1–16] and damage [13–20] by DC electrical resistance measurement. This self-sensing ability is valuable for structural vibration control, weighing, traffic monitoring, border security, building facility management and other applications. It is based on the reversible effect of strain on the volume electrical resistivity (a phenomenon known as piezoresistivity) and the irreversible effect of damage on the resistivity. The strain sensing behavior is such that the resistivity decreases reversibly upon compression (due to the slight push-in of crack-bridging fibers and the consequent decrease of the contact electrical resistivity of the fiber–cement interface) and increases reversibly upon tension (due to the slight pull-out of crack-bridging fibers and the consequent decrease of the contact resistivity), as shown in detail for a curing age of 28 days [2–7,11]. However, the strain sensing behavior changes at a curing age between 14 and 28 days. At 14 days (or less) of curing, the resistivity increases reversibly under both tension and compression, in contrast to the behavior at 28 days (or more) of curing [8].

The self-sensing ability of carbon fiber reinforced cement has been well demonstrated under tension and under compression. However, its demonstration under flexure has been carried out only at 7 days of curing [1]. As flexural loading is commonly encountered by concrete structural components such as slabs, it is important to demonstrate the self-sensing ability at 28 days (or more) of curing.

Flexure involves tension on one side of the specimen and compression on the opposite side. Thus, the prior flexural self-sensing demonstration involved the use of separate

* Corresponding author. Tel.: +1 716 645 2593x2243; fax: +1 716 645 3875.
E-mail address: ddlchung@buffalo.edu (D.D.L. Chung).

0008-6223/$ - see front matter © 2005 Elsevier Ltd. All rights reserved.
doi:10.1016/j.carbon.2005.12.009

electrical contacts on the tension surface and on the compression surface [1], so that the surface resistance (as opposed to the volume resistance) of each surface is monitored during flexure.

In this work, the resistance measurement during flexure is extended to include measurement of the oblique resistance and the through-thickness resistance. The through-thickness direction is in the loading direction, perpendicular to the tension and compression surfaces. The oblique resistance is at an angle between the through-thickness direction and the plane of the tension or compression surface. The resistances in different directions are expected to be sensitive to the strain or damage at different locations of the specimen. Measurement of the oblique and through-thickness resistances involves the use of two electrical contacts on the tension surface and two other contacts on the compression surface. For the through-thickness resistance measurement, the contacts on the two surfaces are directly opposite, with the current contact of one surface opposite that of the opposite surface, and the voltage contact of one surface opposite that of the opposite surface. For the oblique resistance measurement, the contacts on the two surfaces are not directly opposite. In contrast, surface resistance measurement involves all four contacts on the same surface.

In the prior flexural self-sensing demonstration carried out for carbon fiber mortar at 7 days of curing, it was observed that both the tension surface resistance and the compression surface resistance increased upon flexural loading, such that the fractional increase in resistance was larger for the compression surface than the tension surface at the same displacement up to failure [1].

The prior flexural demonstration mentioned above involved carbon fiber reinforced cement mortar (with sand) that contained methylcellulose but no silica fume for helping the fiber dispersion [1]. Silica fume in combination with methylcellulose has since been shown to be the most effective admixture for promoting fiber dispersion [21–24]. Therefore, this paper uses silica fume in combination with methylcellulose in carbon fiber cement.

The prior flexural demonstration mentioned above involved carbon fiber mortar (with sand) [1]. In contrast, this work involves carbon fiber cement paste (without sand). Although aggregates are used in practice, the performance for the case without aggregate provides a reference point for the self-sensing behavior. This reference point is valuable for fundamental understanding of the behavior.

Another prior flexural self-sensing demonstration [16] involved measurement of the volume resistance of the overall specimen rather than the surface resistances of the tension and compression surfaces. The volume resistance was observed to increase monotonically upon flexure up to failure [16]. For both scientific and technological reasons, it is important to study the surface resistance, the measurement of which can be more conveniently implemented on a concrete structure (such as a slab) than the measurement of the volume resistance.

In both Refs. [1,16], the self-sensing was mainly directed at damage sensing, since the effect of reversible strain under flexure was not studied. In contrast, this paper addresses the self-sensing of both strain and damage under flexure, with attention on the effects of both reversible strain and irreversible strain.

Yet another prior flexural self-sensing demonstration involved a plain cement paste (no admixture) substrate with carbon fiber reinforced cement paste (with either latex or silica fume as an admixture) coated on both tension and compression surfaces of the substrate [10]. This demonstration was carried out at 28 days of curing. It shows that the tension surface resistance increases reversibly while the compression surface resistance decreases reversibly upon flexure, as expected for a curing age of 28 days. This demonstration shows that carbon fiber reinforced cement is effective as a strain sensing coating, but it does not demonstrate the flexural self-sensing ability of carbon fiber reinforced cement.

Concrete that is used in load-bearing applications typically contains steel reinforcing bars (i.e., steel rebars). Due to the high electrical conductivity of steel (even more conductive than carbon fiber), there has been concern that the presence of steel rebar may make carbon fiber reinforced cement unable to provide the self-sensing function.

This paper is aimed at investigating the behavior of strain and damage self-sensing in carbon fiber reinforced cement under flexure. A second objective is the investigation of the effectiveness of oblique and through-thickness resistances for indicating strain and damage in carbon fiber reinforced cement. A third objective is to study the effect of steel rebars on the self-sensing ability of carbon fiber reinforced cement.

2. Experimental methods

The carbon fibers were isotropic pitch based and unsized, as obtained from Ashland Petroleum Co. (Ashland, KY). The fiber diameter was 15 μm. The nominal fiber length was 5 mm. Fibers in the amount of 0.50% by mass of cement (corresponding to 0.48 vol%) were used. The percolation threshold is between 0.5 and 1.0 vol% [25]. Prior to using the fibers in cement, they were dried at 110 °C in air for 1 h and then surface treated with ozone by exposure to O_3 gas (0.6 vol%, in O_2) at 160 °C for 10 min. The ozone treatment was for improving the wettability of fibers by water [7].

The cement used was Portland cement (Type I) from Lafarge Corp. (Southfield, MI). The silica fume (Elkem Materials Inc., Pittsburgh, PA, microsilica, EMS 965) was used in the amount of 15% by mass of cement. The methylcellulose, used in the amount of 0.4% by mass of cement, was Dow Chemical Corp., Midland, MI, Methocel A15-LV. The defoamer (Colloids Inc., Marietta, GA, 1010) used whenever methylcellulose was used was in the amount of 0.13 vol% (% of specimen volume).

A rotary mixer with a flat beater was used for mixing. Methylcellulose was dissolved in water and then the defoamer and fibers were added and stirred by hand for about 2 min. Then, the methylcellulose mixture, cement, water and silica fume were mixed for 5 min. After pouring the mix into oiled molds, an external electric vibrator was used to facilitate compaction and decrease the amount of air bubbles. The specimens were demolded after 1 day and then allowed to cure at room temperature in air (relative humidity = 100%) for 28 days. The water/cement ratio was 0.35. Six specimens were tested to confirm the reproducibility of the results of this work.

The specimen configuration for flexural testing (three-point bending at a span of 140 mm) is illustrated in Fig. 1. The specimen was a rectangular beam of size $160 \times 40 \times 40$ mm. Two parallel steel rebars (diameter = 2.95 mm, cross-sectional area = 6.83 mm^2) were embedded in each specimen, such that each rebar extended along the whole length of the specimen (protruding a little out of each of the two end surfaces) and was centered at a plane 5 mm from the bottom surface of the specimen. The cross-sectional view is shown in Fig. 2. Specimens of the same dimensions but without rebar were prepared for comparative testing. Six specimens of each type were tested.

Electrical contacts in the form of silver paint in conjunction with copper wire were applied on the tension and compression surfaces. Contacts A_1, A_2, A_3 and A_4 were on the compression side; contacts B_1, B_2, B_3 and B_4 were on the tension side. Each contact was in the form of a strip in the transverse direction on the tension or compression surface. The various contact strips were parallel to one another.

The compression surface resistance was measured by using A_1 and A_4 as current contacts and A_2 and A_3 as voltage contacts. The tension surface resistance was measured by using B_1 and B_4 as current contacts and B_2 and B_3 as voltage contacts. The through-thickness resistance was measured by using A_1 and B_1 as current contacts and A_2 and B_2 as voltage contacts. The oblique resistance was measured by using A_1 and B_4 as current contacts and A_2 and B_3 as voltage contacts. A voltage supply, a voltmeter and a 1,000 Ω standard resistor (in series with the specimen) were used to measure the DC resistance.

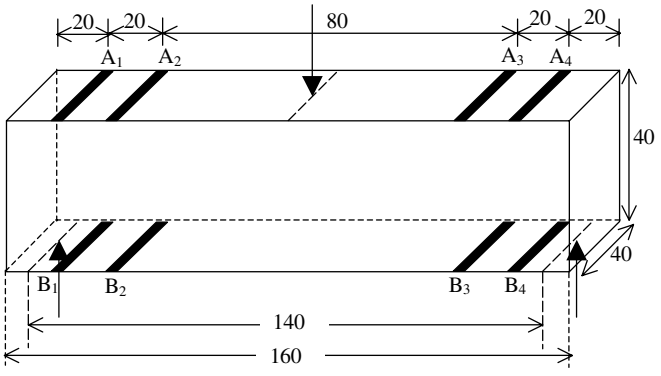

Fig. 1. Specimen configuration for flexural testing by three-point bending. The three points are shown by arrows. A_1, A_2, A_3 and A_4 are electrical contacts on the compression surface, whereas B_1, B_2, B_3 and B_4 are electrical contacts on the tension surface. All dimensions are in mm.

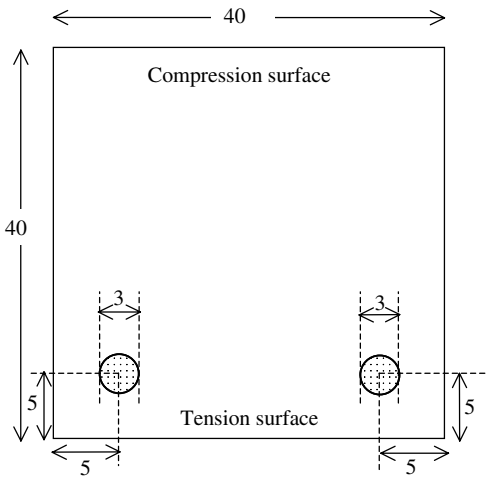

Fig. 2. Cross-sectional illustration of a specimen containing two steel rebars (dotted regions). All dimensions are in mm.

Loading was provided by a hydraulic mechanical testing system (MTS 810), which also provided measurement of the displacement during flexure. Loading was repeatedly applied either at a fixed stress amplitude (i.e., a fixed midspan deflection) or at progressively increasing stress amplitudes. For the case of a fixed stress amplitude, one of two midspan deflections was used. For the midspan deflection of 0.143 mm, the stress amplitude was 1.75 and 2.60 MPa for the cases without and with steel, respectively. For the midspan deflection of 0.215 mm, the stress amplitude was 2.60 and 4.00 MPa for the cases without and with steel, respectively. In the case without rebars, the stress amplitude was increased up to failure for the purpose of studying both strain and damage effects. In the case with rebars, testing was performed only in the elastic regime for the purpose of studying the effect of strain. The four resistances mentioned in the last paragraph were continuously measured, such that the tension and compression surface resistances were measured simultaneously and then the through-thickness and oblique resistances were successively measured, such that the time elapsed between successive measurements was 0.3 s.

3. Results and discussion

3.1. Self-sensing under flexure without steel rebar

This section addresses the self-sensing of strain and damage for the case without rebar. Figs. 3–6 show the fractional change in resistance during flexural loading at progressively increasing deflection amplitudes up to failure for the surface resistance on the compression side, the surface resistance on the tension side, the through-thickness resistance and the oblique resistance, respectively.

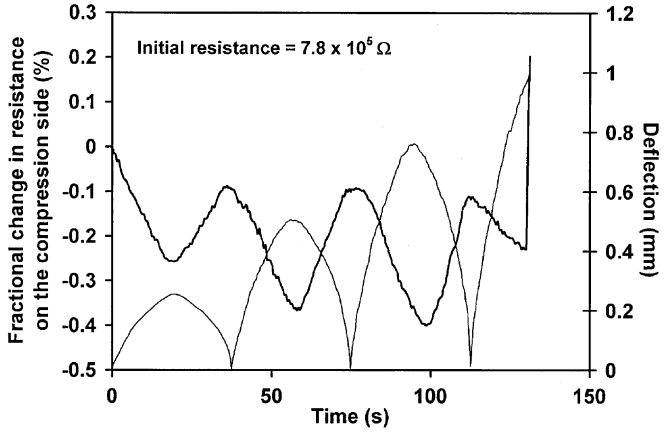

Fig. 3. Fractional change in surface resistance (thick curve) at the compression side vs. time and deflection (thin curve) vs. time during flexural loading at progressively increasing deflection amplitudes up to failure.

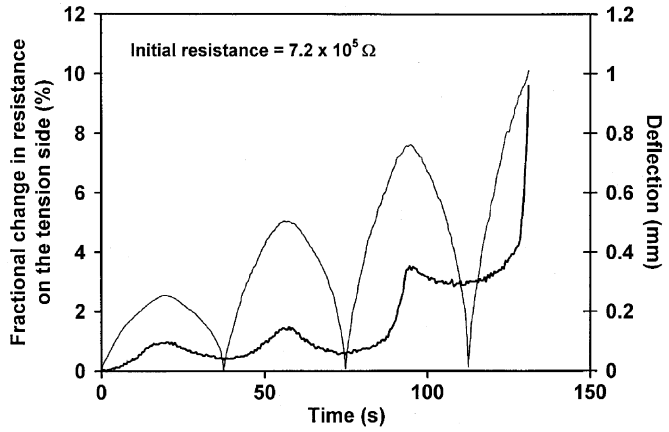

Fig. 4. Fractional change in surface resistance (thick curve) at the tension side vs. time and deflection (thin curve) vs. time during flexural loading at progressively increasing deflection amplitudes up to failure.

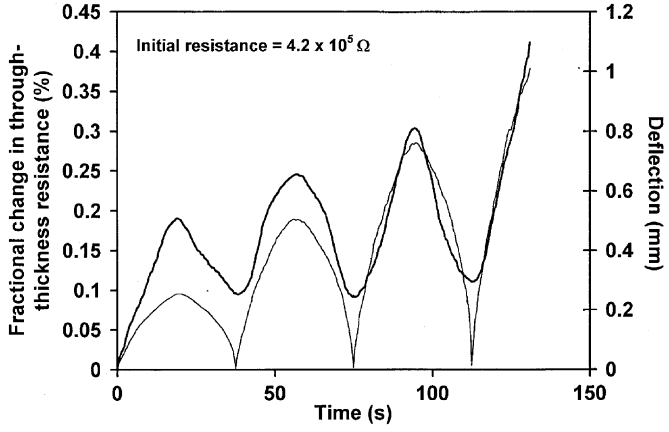

Fig. 5. Fractional change in through-thickness resistance (thick curve) vs. time and deflection (thin curve) vs. time during flexural loading at progressively increasing deflection amplitudes up to failure.

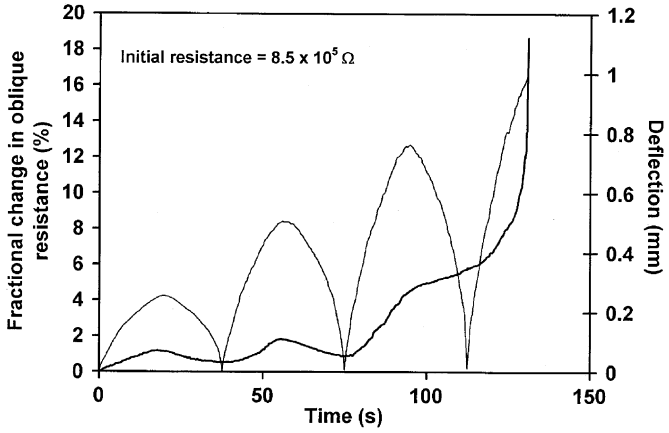

Fig. 6. Fractional change in oblique resistance (thick curve) vs. time and deflection (thin curve) vs. time during flexural loading at progressively increasing deflection amplitudes up to failure.

The surface resistance on the compression side (Fig. 3) decreases upon flexural loading, whereas the surface resistance on the tension side (Fig. 4) increases upon loading. These resistance changes are partly reversible and are due to strain. That the resistance decreases on the compression side and increases on the tension side is consistent with prior results under uniaxial compression [5] and uniaxial tension [6]. The extent of irreversibility increases with the deflection amplitude, due to increasing extent of damage. That damage increases the resistance is consist with prior results under compression [13–17]. At failure, the resistance increases abruptly on both compression and tension sides. The fractional change in resistance, whether due to strain or damage, is much larger in magnitude for the tension side than the compression side.

The through-thickness resistance (Fig. 5) increases upon flexural loading, akin to the behavior of the surface resistance on the tension side. This reflects the much larger fractional change in resistance on the tension side than the compression side. However, the fraction change in through-thickness resistance, whether due to strain or damage, is much smaller than the fractional change in surface resistance on the tension side, because the through-thickness resistance is measured for the part of the specimen that is away from the center, which is the core region of the damage.

The oblique resistance (Fig. 6) increases upon flexural loading, also reflecting the large fractional change in surface resistance on the tension side. However, the fractional change in oblique resistance, whether due to strain or damage, is even larger than that of the surface resistance on the tension side. This large effect on the oblique resistance is attributed to the long current path within the specimen. In contrast, the current path for the through-thickness resistance is short and is located away from the core region of the damage (i.e., away from the center of the specimen along the length). The current path for the surface resistances is quite long, and includes the center part along

the length, but it is restricted to the surface, so that the surface resistances are relatively insensitive to the interior damage.

The extent of irreversibility of the resistance change in the regime of major damage (i.e., the last 1.5 cycles of loading) is greatest for the oblique resistance, less for the surface resistance on the tension side, and least for the surface resistance on the compression side and for the through-thickness resistance. This means that the oblique resistance is most sensitive to damage, the resistance on the tension side is less sensitive to damage, and the resistance on the compression side and the through-thickness resistance are least sensitive to damage.

Fig. 7 shows that the fractional change in resistance per unit deflection is highest for the oblique resistance. The resistance change is quite reversible for the through-thickness resistance and the surface resistance on the compression side (due to the dominance of strain effect), but substantial irreversibility (due to damage) is exhibited by the oblique resistance and the surface resistance on the tension side.

The curve for the oblique resistance (Fig. 7(d)) is unusual in that the resistance upon unloading is lower than that upon loading in the regime of high deflection (above about 0.17 mm), whereas the resistance upon unloading is higher than that upon loading in the regime of low deflection (below about 0.17 mm). This behavior is attributed to the reversible effect due to strain dominating the initial stage of unloading and the irreversible effect due to damage dominating the later stage of unloading. This means that both strain and damage contribute to the overall change in oblique resistance.

The curve for the surface resistance on the tension side (Fig. 7(c)) is such that the initial stage of unloading (a stage that is dominated by the reversible strain effect) is very minor compared to the later stage of unloading (a stage that is dominated by the irreversible damage effect). This means that the overall change in the surface resistance on the tension is mainly due to damage.

The curve for the surface resistance on the compression side (Fig. 7(a)) shows the greatest extent of reversibility among all the curves in Fig. 7. This resistance decreases upon loading, indicating that the resistance change is due to strain rather than damage, which would have caused the resistance to increase upon loading. Thus, the surface resistance on the compression side is the best indicator of strain among the four types of resistances measured in this work.

The above results show that the oblique resistance is the best indicator of the combined effect of strain and damage under flexure. For strain sensing alone, the surface resistance on the compression side is the best indicator. For damage sensing alone, the surface resistance on the tension side is the best indicator.

3.2. Effect of embedded steel rebars

This section addresses the effect of steel rebars on the strain sensing behavior. Figs. 8 and 9 show, for the case with steel, the fractional change in resistance during repeated flexural loading at a midspan deflection of 0.143 mm for the surface resistance on the compression side and the surface resistance on the tension side, respectively. For the case with steel, the initial resistance is very slightly higher for the compression side $[(7.3 \pm 1.1) \times 10^5\ \Omega]$ than the tension side $[(6.4 \pm 0.9) \times 10^5\ \Omega]$. This is due to the proximity of the steel to the tension surface. That the difference is slight means that the current from the tension surface penetrates only slightly into the steel.

The surface resistance on the compression side (Fig. 8) decreases upon flexural loading, whereas the surface resistance on the tension side (Fig. 9) increases upon loading. These resistance changes are totally reversible (except for partial irreversibility after the first loading cycle) and are

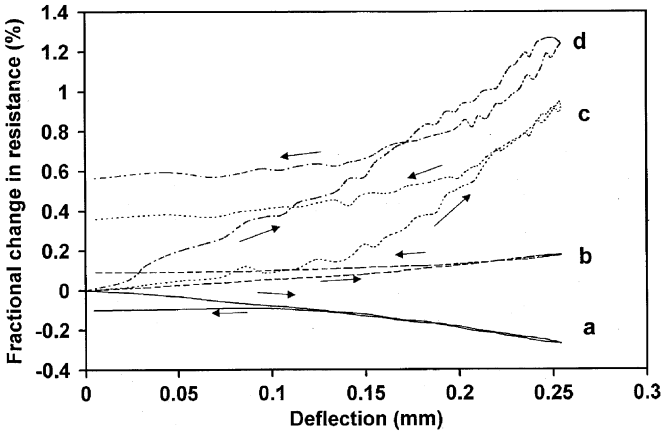

Fig. 7. Fractional change in resistance vs. deflection during loading and unloading in the first loading cycle: (a) surface resistance on the compression side; (b) through-thickness resistance; (c) surface resistance on the tension side; (d) oblique resistance.

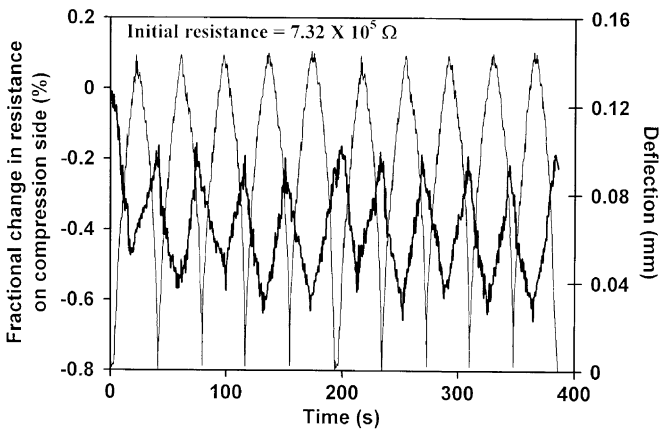

Fig. 8. Variation of the fractional change in resistance on the compression side (thick curve) with time and of the deflection (thin curve) with time during repeated flexural loading at a midspan deflection of 0.143 mm for carbon fiber cement with embedded steel.

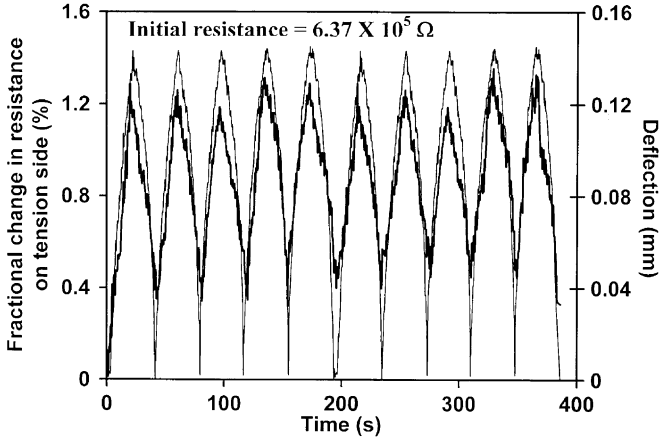

Fig. 9. Variation of the fractional change in resistance on the tension side (thick curve) with time and of the deflection (thin curve) with time during repeated flexural loading at a midspan deflection of 0.143 mm for carbon fiber cement with embedded steel.

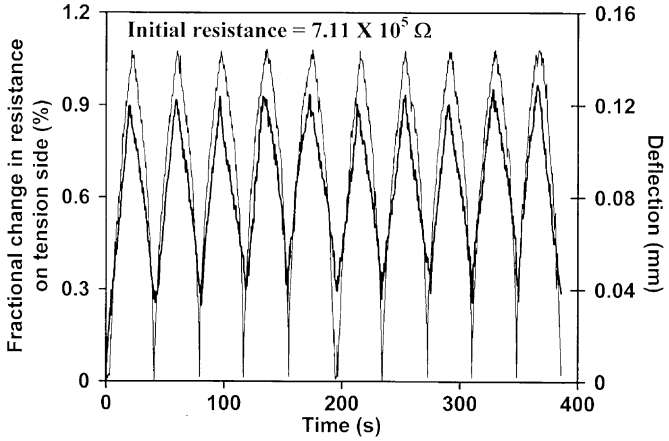

Fig. 11. Variation of the fractional change in resistance on the tension side (thick curve) with time and of the deflection (thin curve) with time during repeated flexural loading at a midspan deflection of 0.143 mm for carbon fiber cement without embedded steel.

due to strain. That the resistance decreases on the compression side and increases on the tension side is consistent with prior results under uniaxial compression [5] and uniaxial tension [6]. The irreversibility is probably due to minor damage, which may be in the form of fiber–matrix debonding on the tension side causing an irreversible resistance increase [19], and increased fiber–fiber contact on the compression side causing an irreversible resistance decrease [18]. The fractional change in resistance, whether due to strain or damage, is much larger in magnitude for the tension side than the compression side.

Figs. 10 and 11 show corresponding results for the case without steel, also at a midspan deflection of 0.143 mm. The initial resistance is $(7.6 \pm 0.8) \times 10^5\ \Omega$ and $(7.1 \pm 0.9) \times 10^5\ \Omega$ for the compression and tension sides, respectively. These values are essentially the same, as expected, since steel is absent. Comparison of the corresponding values with and without steel shows that the steel decreases the surface resistance of the tension side slightly and essentially does not affect that of the compression side.

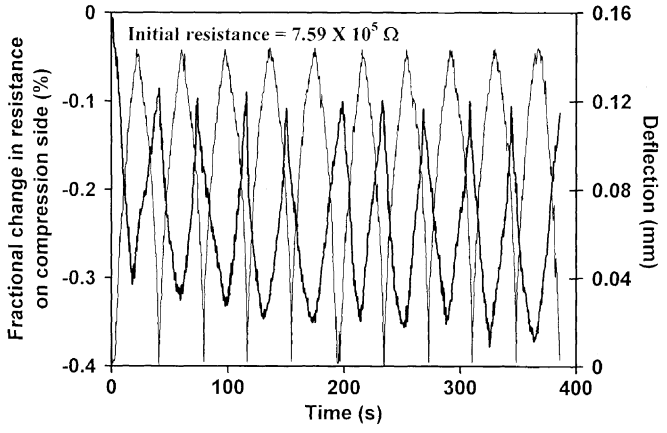

Fig. 10. Variation of the fractional change in resistance on the compression side (thick curve) with time and of the deflection (thin curve) with time during repeated flexural loading at a midspan deflection of 0.143 mm for carbon fiber cement without embedded steel.

Table 1
Ratio (10^{-2} mm^{-1}) of the peak value of the fractional change in surface resistance to the midspan deflection

Midspan deflection (mm)	Surface	Without steel	With steel
0.143	Tension	6.5 ± 0.8	9.3 ± 1.2
0.143	Compression	-2.4 ± 0.8	-4.1 ± 0.5
0.215	Tension	6.9 ± 0.8	9.6 ± 1.1
0.215	Compression	-2.6 ± 0.3	-4.3 ± 0.5

Table 1 shows that the strain sensing effectiveness, as described by the ratio of the peak value of the fractional change in resistance to that of the midspan deflection, is larger (by 40%) in the presence of steel for the tension side. The magnitude is increased by 70% in the presence of steel for the compression side. These differences between the cases with and without steel occur for both midspan deflections.

That the presence of steel causes the ratio (Table 1) for the tension side to be higher is because of the slight penetration of the current into the steel and the increasing difficulty of this penetration upon deflection (due to slight loosening of the steel–cement interface upon deflection). The difficulty of penetration causes the measured surface resistance to increase. This effect is reversible, except for partial irreversibility in the first loading cycle (Figs. 9 and 11). It is in addition to the piezoresistive effect of carbon fiber cement. The piezoresistive effect also causes the resistance to increase on the tension side. These two effects in combination result in an increase of the ratio (Table 1) relative to the case without steel.

That the presence of steel causes the ratio for the compression side to be higher in magnitude is because, at the same midspan deflection, the stress is higher for the case with steel. The higher stress causes more local deformation at the compression side, which is away from the rebar. The

greater deformation gives rise to more resistance change on the compression side, relative to the case without steel, thus resulting in a higher magnitude of the ratio.

Table 1 shows that carbon fiber reinforced cement with embedded steel is effective for the self-sensing of flexural strain. For the same deflection, the steel causes the sensitivity to be higher, whether the resistance is that on the tension side or that on the compression side.

This paper provides the first study of the effect of embedded steel on the self-sensing ability of carbon fiber reinforced cement. The result of this study shows that the steel enhances the self-sensing ability. However, this enhancement also means that the relationship between strain (deflection) and resistance will need to be established by calibration for each configuration of steel prior to using the self-sensing function. Since calibration is expected to be performed for a given structure prior to sensing usage, whether steel rebars are present or not, the calibration requirement does not deter the self-sensing implementation in the presence of steel rebars.

4. Conclusion

Self-sensing of damage and strain is effective in carbon fiber reinforced cement under flexure. The self-sensing is attained by measuring the volume resistance or surface resistance. Electrical contacts are on the compression and/or tension surfaces. The four-probe method is used.

The oblique resistance, which increases upon loading, is a good indicator of the combined effect of damage and strain, whereas the surface resistance (on the compression side), which decreases upon loading, is a good indicator of strain alone. The surface resistance (on the tension side), which increases upon loading, is a good indicator of damage alone. The through-thickness resistance, which increases slightly upon loading, is a relatively poor indicator of both strain and damage, due to its region of measurement being away from the core of the damage. In contrast, the oblique resistance and the surface resistances on tension and compression sides are associated with a region of measurement that includes the core of the damage.

The self-sensing ability of carbon fiber reinforced cement, as shown for the sensing of flexural strain, is enhanced by the presence of embedded steel. The fractional change in surface electrical resistance is increased by 40% on the tension surface of the specimen under three-point bending, due to the steel. The magnitude of the fractional change in surface resistance is increased by 70% on the compression surface, due to the steel.

Acknowledgment

This work was supported in part by US National Science Foundation.

References

[1] Chen P-W, Chung DDL. Concrete as a new strain/stress sensor. Composites Part B 1996;27B:11–23.
[2] Chung DDL. Piezoresistive cement-based materials for strain sensing. J Intel Mater Syst Struct 2002;13(9):599–609.
[3] Wen S, Chung DDL. A comparative study of steel- and carbon–fibre cement as piezoresistive strain sensors. Adv Cem Res 2003;15(3):119–28.
[4] Chung DDL. Electrical conduction behavior of cement–matrix composites. J Mater Eng Perf 2002;11(2):194–204.
[5] Wen S, Chung DDL. Uniaxial compression in carbon fiber reinforced cement, sensed by electrical resistivity measurement in longitudinal and transverse directions. Cem Concr Res 2001;31(2):297–301.
[6] Wen S, Chung DDL. Uniaxial tension in carbon fiber reinforced cement, sensed by electrical resistivity measurement in longitudinal and transverse directions. Cem Concr Res 2000;30(8):1289–94.
[7] Fu X, Lu W, Chung DDL. Ozone treatment of carbon fiber for reinforcing cement. Carbon 1998;36(9):1337–45.
[8] Fu X, Chung DDL. Effect of curing age on the self-monitoring behavior of carbon fiber reinforced mortar. Cem Concr Res 1997;27(9):1313–8.
[9] Chen P-W, Chung DDL. Carbon fiber reinforced concrete as a smart material capable of non-destructive flaw detection. Smart Mater Struct 1993;2:22–30.
[10] Wen S, Chung DDL. Carbon fiber-reinforced cement as a strain-sensing coating. Cem Concr Res 2001;31(4):665–7.
[11] Wen S, Chung DDL. Strain sensing characteristics of carbon fiber cement. ACI Mater J 2005;102(4):244–8.
[12] Sun M, Mao Q, Li Z. Size effect and loading rate dependence of the pressure-sensitivity of carbon fiber reinforced concrete (CFRC). J Wuhan Univ Tech, Mater Sci Ed 1998;58–61.
[13] Mao Q, Zhao B, Sheng D, Li Z. Resistance changement of compression sensible cement speciment under different stresses. J Wuhan Univ Tech 1996;11(3):41–5.
[14] Reza F, Batson GB, Yamamuro JA, Lee JS. Resistance changes during compression of carbon fiber cement composites. J Mater Civil Eng 2003;15(5):476–83.
[15] Wu Y, Bing C, Keru W. Smart characteristics of cement-based materials containing carbon fibers. Mech Mater Eng Sci Exp 2003:172–175.
[16] Yao W, Chen B, Wu K. Smart behavior of carbon fiber reinforced cement-based composite. J Mater Sci Technol 2003;19(3):239–43.
[17] Bontea D-M, Chung DDL, Lee GC. Damage in carbon fiber reinforced concrete, monitored by electrical resistance measurement. Cem Concr Res 2000;30(4):651–9.
[18] Fu X, Chung DDL. Self-monitoring of fatigue damage in carbon fiber reinforced cement. Cem Concr Res 1996;26(1):15–20.
[19] Chung DDL. Damage in cement-based materials, studied by electrical resistance measurement. Mater Sci Eng R 2003;42(1):1–40.
[20] Wen S, Chung DDL. Effects of strain and damage on the strain sensing ability of carbon fiber cement. J Mater Civil Eng [in press].
[21] Chung DDL. Improving cement-based materials by using silica fume. J Mater Sci 2002;37(4):673–82.
[22] Chung DDL. Dispersion of short fibers in cement. J Mater Civil Eng 2005;17(4):379–83.
[23] Cao J, Chung DDL. Carbon fiber reinforced cement mortar improved by using acrylic dispersion as an admixture. Cem Concr Res 2001;31(11):1633–7.
[24] Fu X, Chung DDL. Combined use of silica fume and methylcellulose as admixtures in concrete for increasing the bond strength between concrete and steel rebar. Cem Concr Res 1998;28(4):487–92.
[25] Chen P-W, Chung DDL. Improving the electrical conductivity of composites comprised of short conducting fibers in a non-conducting matrix: the addition of a non-conducting particulate filler. J Elect Mater 1995;24(1):47–51.